About the 3D Simulation of the Boiling of Liquid Films and Spray Droplets During their Contact with Hot Substrates

Chaouki Habchi

DOI
10.1007/s00231-022-03222-1

About the 3D simulation of the boiling of liquid films and spray droplets during their contact with hot substrates

Chaouki Habchi

IFP Energies nouvelles, Institut Carnot IFPEN Transports Energies,

1 et 4 avenue de Bois-Préau, 92852 Rueil-Malmaison, France

Corresponding author Chaouki.Habchi@ifpen.fr

ORCID: https://orcid.org/0000-0002-6234-3434

Highlights

1- Clarify the state of the art on the 3D simulation of the boiling of liquid films and spray droplets during their contact with hot substrates.
2- Propose updated set of heat transfer models and correlations for spray-wall interaction regimes while considering liquid film boiling and conjugate heat transfer (CHT).
3- Propose a detailed analysis and experimental validation for the simulated cooling of the wall surface and the evolution of the heat flux during the impact of a spray on a heated wall.

Abstract

Boiling of liquids upon impact of the spray on heated surfaces is common in many practical applications. However, a comprehensive modelling approach for these phenomena is still not available in commercial software, despite decades of experimental, theoretical, and numerical research efforts. The motivation of this paper is to clarify the state of the art on the three-dimensional (3D) simulation of the boiling of liquid films and spray droplets during their contact with hot substrates. Based on recent experimental and theoretical research, this paper proposes a set of heat transfer models for 3D simulation of spray cooling considering conjugate heat transfer (CHT). These updated models and correlations were implemented in a computational fluid dynamics (CFD) solver, which already included a classical two-phase Lagrangian-Eulerian approach and CHT modelling functionality. A detailed validation of the improved modelling proposals is performed

using a unique and novel database including wall surface temperature and heat flux measurements for different flow rates and spray impact velocities. Excellent agreement with experiments was obtained for all boiling regimes using a Leidenfrost-like temperature to manage the prompt heat flux change between the film boiling regime and the transition boiling regime. Most notable are the great results produced by the recent film boiling model summarized in this article.

Keywords

Spray cooling, liquid film boiling, conjugate heat transfer, Leidenfrost point.

Introduction

Spray and drop impact on heated surfaces are common in several practical applications: these include electric motors and inverters cooling, internal combustion engines, gas turbines, exhaust urea-water solution technique, for instance. The classification of spray impact regimes is still somewhat controversial, due to the complexity of phenomena observed during spray impact on heated surfaces [1,2]. Because of limited computational resources, historically speaking, most previous computational fluid dynamics (CFD) research has been focused on determining the effects of various factors on the size and velocity distributions of secondary droplets after impact [3-5]. As a result, few models have been designed to allow for a complete numerical solution of conjugate heat transfer (CHT) during spray impact on the one hand and for already formed liquid wall films on the other. This work therefore aims to propose such a new model based on the most recent experimental and theoretical investigations discussed below.

1- Background

Transitions between heat transfer impact regimes were studied mostly from an empirical point of view. Besides, apparent contradictions can be found in the literature, about which parameters govern wall heat transfer at spray impact, as analysis shows that the accuracy of often used empirical correlations strongly depends on the experimental conditions. Among the physical processes experimentally established is that by increasing the wall temperature (T_w), a sessile drop have been seen to transition from the totally wetted evaporation regime, to the nucleate boiling regime, then it transitions to the film boiling regime where the droplet levitates upon a vapour layer (see [6] and the references cited therein). The above description is supported by various experimental observations (see [12, 13, 28, 29], for instance). Classically, in addition to the single-phase regime, at least three thermal regimes are distinguished, which are classified according to the extent of superheating of the wall ($T_w - T_{sat}$) and using as limits for these regimes, the saturation temperature (T_{sat}), the Nukiyama temperature (T_N), and the Leidenfrost temperature (T_L), as shown in Figure 1. However, these temperature thresholds (T_N and T_L) have not been clearly identified because of the high number of possible driving parameters. Nevertheless, few values and correlations have been gathered in [6], for instance. As with a sessile drop, spray cooling also involves a succession of heat transfer regimes: film boiling, film transition boiling, nucleated film boiling, and single-phase liquid film evaporation, each with unique heat transfer characteristics. Because of huge differences in heat transfer values between regimes, cooling proceeds progressively at drastically different rates, as schematically shown in Figure 1(b). First, film boiling is dominated by the formation of a vapour layer along the

entire hot surface. Because of very low thermal conductivity of vapour, cooling rate in film boiling is quite slow. Within the transition boiling regime, liquid contact ensues with portions of the surface (while other portions continue to endure film boiling), which causes appreciable improvement in heat transfer up to the critical heat flux (CHF). Then, the nucleate boiling regime is marked by abundance of vapour bubbles nucleating, growing, and departing from the surface at high frequency, thereby providing the best heat transfer up to CHF, and therefore fastest wall cooling rate, of all four regimes. These regimes are qualitatively identifiable with the aid of the boiling curve, as explained previously by the author in [6]. However, much research efforts are still needed due to the lack of universal accurate models for the various heat transfer regimes and their temperature thresholds. By investigating the boiling curve of sessile droplets deposed on various heated wall materials, Liu et al. [9] highlighted that the minimum evaporation time (i.e. at T_N) corresponds usually to a range of temperature, which may extent up to 20K. In addition, the experimental results have shown the high variation of the Nukiyama temperature with the wall materials [9,10]. Besides, among the many mechanisms important to spray cooling, Leidenfrost point (LFP) represents a crucial transition point having appreciable impact on wall cooling by the fuel spray impingement, particularly in internal combustion engines, as discussed in [6], for instance. A brief review of the mechanisms that significantly affect the LFP is collected here: the Leidenfrost temperature increases when the ambient pressure [6, 12], the drop impact velocity [13] and the initial wall temperature increase [14]. However, it decreases when the impact mass flow rate is increased [14]. In addition, Cai et al. [11] have shown clearly that LFP temperature increases with increasing surface roughness. Besides, Park & Kim [15] have observed that when single droplets dynamically collide with a heated surface during film boiling above the LFP, small spots of higher heat flux due to localized wetting during the collision appear as increasing the impact Weber number. A systematic comparison of their experiments revealed that existing theoretical models do not consider these observed physical phenomena which may lead to inaccurate simulations. Vapour cooling of poorly conducting hot substrates have been shown to be another physical phenomenon that increases the dynamic Leidenfrost temperature [16]. Although considerable experimental databases on LFP have been reported in the previous literature for different fluids, wall materials and surface roughness, etc., only a small subset of these studies have convincingly captured the underlying physical mechanism responsible for LFP initiation, which is an essential starting point for building any predictive model. Recently, a theoretical model was proposed to estimate the minimum temperature required for a droplet to rebound at different impact conditions [17]. This new model for the dynamic Leidenfrost temperature ($T_{L,d}$) is very promising because it is the first to involve the wall effusivity, (defined as, $e_w=(\rho\lambda c_p)^{1/2}$ where ρ is density, λ is the thermal conductivity, and c_p the specific heat) and implicitly accounts for the ambient pressure effect. However, this model is still not accurate enough as it does not include various important well-known effects such as the wall surface structure. Therefore, no reliable estimates of (T_L) and ($T_{L,d}$) are available so far. For this reason, most CFD solver use the $T_{L,d}$ value as a user input, often hidden in the spray-wall interaction map critical parameter ($T^*_{crit} = T_{L,d}/T_{sat}$). Therefore, to determine the actual thermal regime for an impinging drop, the model operates by comparing the dimensionless wall temperature ($T^* = T_w/T_{sat}$) value to the given critical temperature threshold, T^*_{crit}. In this work, this (T*)-criterion is used.

Therefore, no liquid film is formed on the wall, as discussed above in the case ($T^* > T^*_{crit}$). However, a specific heat flux is exchanged between the impinging droplets and the wall. To estimate this heat flux, most of the CFD solvers, such as StarCD [18] and CONVERGE [19] rely on the Wruck model [20].

This model uses an overestimated contact time and area for the heat flux calculation. Indeed, based on recent experiments from Castanet et al. [21], it has been clearly observed that the characteristic contact time, during which there is a significant heat flux, is much smaller (about ¼) than the total contact time considered in the Wruck model [20]. Consequently, overestimated wall heat flux is obtained, which may induce numerical instabilities. Therefore, an effort should be made to update such modelling based on recently published experimental and theoretical models. In this work, the film boiling model developed by Breitenbach et al. [22] will be implemented and validated.

On the other hand, a liquid film is formed on the wall in the case ($T^* < T^*_{crit}$), for which a specific heat flux is computed depending on whether the wall thermal conditions are found in film boiling, transition boiling, nucleated boiling regime, or it is in single-phase liquid film evaporation regime. The actual wetted regime is determined using T_{sat} and T_N thresholds, as explained in [6,14] for instance. Currently, most of commercial software rely on very old correlations developed for the prediction of pool-boiling heat fluxes. In particular, the (Rohsenow, 1952) [23] correlation is applied for the computation of the heat flux in the nucleate boiling regime, the (Lienhard & Dhir, 1973) [24,25] correlation is applied to the computation of the critical heat flux (CHF) and the (Zuber, 1959) [24] correlation, also obtained in pool boiling conditions, is applied for the computation of the minimum heat flux at (T_L). Therefore, these correlations summarized in Section 3 need to be applied with caution. In the absence of appropriate models in the literature for the nucleate and transition boiling regimes, this paper will use the above-mentioned correlations, but updated by recent experimental data from [14].

2- Objective and organization

The objective of this paper is therefore to design a complete numerical solution of the conjugate heat transfer (CHT) between the spray and the wall during the spray impact, but also for the already formed liquid wall films. More specifically, this work aims to evaluate the film boiling model proposed recently in [22] and to propose a set of updated correlations, experimentally validated for the rest of the boiling regimes. The validation will be mainly based on a unique and recently published experimental database in terms of wall surface temperature and heat flux evolution during spray impact on heated walls [14].

The rest of this article is organized as follows: first, an updated set of heat transfer models and correlations covering the different liquid film regimes will be summarized in Section 3. The implementation of the above set of models in the CONVERGE CFD solver is then explained in Section 4. Section 5 describes the experimental database of Tenzer et al. [14] and the numerical configuration of the cases used in Section 6 for models' validation and numerical results analysis. Finally, the numerical and experimental results are compared and discussed before conclusions and recommendations for future work.

3- Heat transfer models and correlations

This paper focuses on the study and evaluation of an updated set of correlations for the calculation of wall heat flux between the wall surface and the liquid film in the nucleate boiling, transition boiling, and Leidenfrost boiling regimes. Next, a new model recently developed by Breitenbach et al.

[22] for the calculation of the wall-surface heat flux upon impact of the spray droplets on a heated wall in the film boiling regime is summarized.

3.1 Liquid film boiling

Figure 2 shows the updated wall heat flux models compared to the one previously used in the CONVERGE CFD solver, for a liquid film already formed on the wall. In this figure, q_{film} is the conduction heat flux when the liquid film is completely wetting the wall around (T_{sat}). q_{min} and q_{max} are the wall heat flux at (T_L) (i.e. at the static Leidenfrost temperature) and the critical heat flux (CHF) calculated respectively by Zuber [24], Eq. (1), and Lienhard & Dhir [24,25], Eq. (2).

$$q_{min} = C_1\, \rho_g L \left[\frac{\sigma\, g\, (\rho_l - \rho_g)}{(\rho_l + \rho_g)^2}\right]^{0.25} \tag{1}$$

$$q_{max} = C_2 \sqrt{\rho_g}\, L\left[\sigma\, g\, (\rho_l - \rho_g)\right]^{0.25} \tag{2}$$

$$q_{nb} = \mu_l\, L \sqrt{g\, \left(\frac{\rho_l - \rho_g}{\sigma}\right)}\, \left[\frac{C_{p,l}(T_w - T_{sat})}{C_{sf}\, L\, Pr^s}\right]^3 \qquad \text{with} \qquad Pr = \frac{\mu_l\, C_{p,l}}{\lambda_l} \tag{3}$$

In the above equations, the subscript (l) ang (g) stand for liquid and gas, g is the gravity, (ρ_g) is the local gas density in the wall-cell. The liquid latent heat of vaporisation (L), the surface tension (σ) and the liquid density (ρ_l) and viscosity (μ_l) are computed at (T_{sat}). The original coefficient values are ($C_1 = 0.09$) and ($C_2 = 0.149$). However, these coefficients depend on several parameters, as discussed in [24,25], and they are considered in this work as user parameters. Indeed, the values ($C_1 = 0.09 * 10$) and ($C_2 = 0.149/2$) have been selected to compare better with the experiments of Tenzer et al. [14], as discussed below in Section 6.

The Rohsenow correlation [23,24] given by Eq. (3) is usually applied to compute the heat flux (q_{nb}) in the nucleate boiling regime. The original values of its parameters are ($C_{sf} = 0.006$) and ($s = 1$) have not been modified in this work. However, it is recommended to make then as user parameters for better accuracy with different liquids and walls.

One can see in Figure 2 (red curve) that the Rohsenow correlation, Eq. (3) has been found to give much higher heat flux at CHF when compared to (q_{max}) given by Eq. (2). Because of this non consistent discontinuity, Eq. (3) has been only used for the estimation of q_{film} while assuming an initial superheat of 5K. This value is arbitrary, but it is a practical choice that allows to compute q_{film} with ($T_w = T_{sat} + 5K$) in Eq. (3).

Next, a linear interpolation between q_{film} and q_{max} is proposed (green line) in the nucleate boiling regime. Moreover, the CHF (i.e. at T_N) corresponds experimentally to a range of temperature, which has been found experimentally to extent up to 20K, as discussed by Liu et al. [9]. Therefore, the updated CHF, Eq. (2) is applied in the present work in a range of wall temperature of 20K between T_N and $T_{N,max}$, as depicted in Figure 2 (in green) with ($T_N = 0.25 * [T_{sat} + 3T_L]$) and ($T_{N,max} = T_N + 20K$).

A linear interpolation between q_{max} and q_{min} is also used in the transition boiling regime, as shown in Figure 2.

Finally, when the liquid film moves to a wall surface greater than (T_L), the liquid film should completely levitate above the wall. In this condition, the liquid film should be released into spray parcels with smaller droplets, as observed experimentally in [9] for instance. However, this thermal breakup has not been implemented in the current work and the heat flux for liquid film in the Leidenfrost regime is simply computed using again a linear interpolation, Eq. (4), similar to previous modelling, such as in StarCD [18,26] and CONVERGE CFD [19] solvers.

$$q_{leiden} = q_{min} \left(\frac{(T_w - T_{sat})}{(T_L - T_{sat})}\right) \quad (4)$$

It worth to mention that this new implementation has been inspired from the existing experimental and theoretical works reviewed above in the Background Section.

3.2 Wall Heat flux of spray droplets impacting a heated wall in the film boiling regime

The current work is based on the film boiling model recently published by the group of Prof. Tropea in Darmstadt [22]. More precisely, the model accounts for the main physical phenomena: development of thermal boundary layers in the liquid and solid regions, liquid evaporation, and creation of an expanding vapour layer. Further, thermal effusivity of the droplet and the wall are taken into account including relevant material properties, *defined as* $e_k=(\rho\lambda c_p)_k^{1/2}$ where ρ is the density, λ is the thermal conductivity, and c_p the specific heat of the wall (*index k=wall*) and the liquid droplet (*index k=liquid*).

The model allows estimation of the total heat Q_{single}, Eq. (5) collected by a single drop during its spreading and receding on a hot substrate. The heat removed by a single impacting drop during the initial stage time of drop spreading and up to ($t_i = D_0/U_0$) is first derived, where D_0 and U_0 are the impact droplet diameter and wall normal velocity, respectively. This first part of the theoretical derivation is consistent with various experiments and particularly with those of Castanet et al. [21], in which it has been clearly observed that the contact time, during which there is a significant heat flux, is much smaller (about ¼) than the total contact time $4*D_0/U_0$ estimated also experimentally. The reader may refer to Figure 3 in [17] for more details. In the current article, a correction factor β is introduced to account the rest of the drop spreading and for possible droplets interaction during their spreading on Q_{single} given by Eq. (5):

$$Q_{single} = \beta \frac{4.63\, D_0^{5/2}\, G\, e_w\, (T_w - T_{sat})}{U_0^{1/2}\, (K+2\,G)} \quad (5)$$

Where

$$K = \sqrt{(B-G)^2 + \frac{4G}{\sqrt{\pi}}} - B - G \quad , \quad G = \frac{\sqrt{\pi}\,\lambda_v\,\rho_l L}{2(T_w - T_{sat})e_w^2} \quad , \quad B = \frac{\sqrt{5}\,(T_{sat} - T_{Do})\,e_l}{\sqrt{\pi}\,(T_w - T_{sat})\,e_w}$$

(ρ_l) is the liquid density, (λ_v) is the vapour thermal conductivity and (L) the liquid latent heat of vaporisation, both calculated at the mean vapour layer temperature, ($T_v=0.5*[T_w+T_{sat}]$) where the lower surface side of the drop is assumed at T_{sat}. Based on the different simulations performed below (Section 6), the value of β has finally be selected equal to 0.65 for all the simulations in the present article.

4- Models implementation

The proposed updated set of heat transfer models and correlations have been implemented in the CONVERGE CFD solver [19]. This software already includes a comprehensive set of Eulerian-Lagrangian spray and liquid film models with a CHT functionality. Therefore, interested readers could refer to [19] for a detailed description of the previously existing models in CONVERGE. First, the heat flux correlations summarized by equations (1)-(4) have been implemented as an update of the liquid film model described in the CONVERGE manual [19]. Next, the model given by Eq. (5) for the calculation of the heat flux in the film boiling regime has been implemented in a way similar to the Wruck model [19,27] in the dynamic wall-spray interaction model of Kuhnke [19,20]. More specifically, this model is applied only when (T_w > $T_{L,d}$), where T_w is the most updated wall temperature obtained using the conjugate heat transfer (CHT) method. Because the dynamic Leidenfrost temperature ($T_{L,d}$) is unknown, its value at atmospheric pressure is considered as an input value for the simulations, following the (T^*_{crit})-ratio approach, as explained in the Background Section. Then, ($T_{L,d}$) value at the current pressure may be estimated using the author correlation given in [6].

5- Models validation

5.1 Validation experimental database

Figure 3 shows the main characteristics of the Darmstadt experiments [14]. The experimental set-up was designed for spray cooling characterization using various techniques. Interested readers should refer to the latter reference for the detailed description of the experimental techniques. The impacting spray is described mainly by the injected water initial temperature, (T_{f0}) and three local properties measured at the wall surface location: impact mass flux density ($\dot{m}$), impact mean drop diameter, (D_{10}) and impact mean drop velocity, (U). It is interesting to note that these properties have been found nearly uniform close to the centre of the substrate (see figure 3 in [14]). The operating and boundary conditions gathered from [14] are summarized in Figure 3(a) and listed in Table 1 along with the main experimental results range values.

5.2 Computational framework

In this work, the CONVERGE CFD solver [19] is used as the computational framework for simulating the Darmstadt experiments [14]. CONVERGE is a general purpose CFD code for the calculation of three-dimensional, incompressible, or compressible, chemically reacting fluid flows in complex geometries with stationary or moving boundaries. This code can handle an arbitrary number of species and chemical reactions, as well as transient liquid sprays, and laminar or turbulent flows. CONVERGE generates the Cartesian grid internally at runtime. This process involves refining any embedding in specified locations and times, and Adaptive Mesh Refinement (AMR) to automatically change the grid based on different specified criteria for adding grid resolution where it is most useful.

Figure 4 highlights the different grid refinement at t=20s for Case 7 ($\dot{m}$ = 2.9 kg/m^2/s and U = 10.3 m/s, as depicted in Table 2) on a 2D-cut of the 3D mesh used in this study. The base grid is equal to 4 mm in the solid region and 1 mm in the gas region. Three fixed embedding were specified. The first one with 0.5 mm grid size is located downstream of the injector nozzle (at the top, as shown in Figure 4). The other two, with a 0.25 mm grid, aim to resolve the thermal boundary layer on either side of

the substrate surface. In addition, AMR is classically used in the spray region based on a minimum velocity gradient criterion to optimize the two-way coupling of the spray droplets with the gas. This refinement strategy used together with a RANS (Reynolds-averaged-Navier-Stokes) solver with a standard (K-ε) turbulence model and a Lagrangian approach for two-phase spray modelling, proved to be sufficiently accurate when the numerical results are compared below to the experimental data. Finally, it is worth to mention that with the current refinement strategy, the total number of cells is between 5 and 9 million during runtime. The CPU time is 765 seconds per second computed on 360 cores of the latest generation Intel Skylake G-6140 processors running at 2.3 GHz (ENER440 IFPEN Supercomputer).

5.3 Numerical stability of the boiling model

For numerical stability and physical consistency, the CFD time step (dt) should be greater than the initial impact contact time ($t_i=D_0/U_0$) assumed for the derivation of Eq. (5) in [22]. Otherwise, the total heat (Q_{tot}) collected by the droplets impacting the face of a wall cell is going to be overestimated and may lead to some numerical instabilities. One way to avoid this issue is to estimate the number of CFD time-steps N = int(t_i/dt) to be used to resolve temporally the current heat flux Q_{tot}. Therefore, care should be made for the case N>1. For the present simulations, t_i is found equal to 5 µs (because $D_0\approx$ 50 µm and $U_0\approx$ 10 m/s, as could be seen in Table 2) and dt is fixed equal to 500 µs. Therefore, N<<1 for all simulations performed in this paper, which guaranteed the stability of the simulations.

5.4 Numerical setups

Among the available experimental results, seven test cases are simulated. The corresponding parameters and boundary conditions are listed in Table 2, including the dynamic Leidenfrost temperature ($T_{L,d}$) at atmospheric pressure. In the experiments, the magnitude of the impact flow rate, ($\dot{m}$) was varied by changing the injection pressure, and the distance between the nozzle and the wall target. Therefore, before each simulation case, several short simulations were performed to adjust the impact velocity, (U) and mass flow rate ($\dot{m}$) to the considered nominal experimental values. This preliminary setup adjustment is done by trial and error using the nozzle diameter and the injection mass flow rate as parameters. As a matter of fact, ($\dot{m}$) and (U) of impacting droplets are averaged during the runtime on the central disc, depicted in red in Figure 3(b). Figure 5 presents the results of these preliminary simulations, showing a relatively good match with the experimental impact conditions for cases ($\dot{m}$ = 1.6 kg/m^2/s, U = 8 m/s) and ($\dot{m}$ = 0.9 kg/m^2/s, U = 9.9 m/s). Besides, the spray cone angle is 45 degrees and a uniform injection drop size distribution is specified with the Sauter mean diameter, SMD which is found to be close to the measured D_{10} listed in Table 2. Note that since the injection is performed in cold air (Table 1), the droplet size does not decrease too much before the impact of the spray on the heated substrate, even if the droplets evaporation model is activated. Finally, the evaporation of the liquid film is also obviously activated using the updated correlations, Eqs. (1)-(4).

6- Results discussion

For the seven test cases simulated, the numerical mean heat flux and wall surface temperature are compared to the experimental results [14]. The numerical mean heat flux is obtained by averaging all the heat fluxes of the wall cells impacted at each time-step on the central disk (in red in Figure 3(b)). The heat flux in the film boiling regime (when $T_w > T_{L,d}$) is computed using Eq. (5). Then, when the substrate is cooled so that (T_w) becomes less than ($T_{L,d}$), the updated set of correlations, Eqs. (1)-(4) are used to calculate the heat flux due to the wall liquid film in the different regimes, namely nucleate boiling, transition boiling and liquid film Leidenfrost boiling regimes.

6.1 Effects of liquid injection temperature

The influence of the initial spray water temperature (T_{f0}) on the heat flux and surface temperature dependence on time are depicted in Figure 6 for cases 4, 5 and 6 (Table 2). Excellent agreement with experiments was obtained in these cases. The first point to note in Figure 6 is the ability of the film boiling model, (Eq. (5)) to predict sub-cooling effects of the injected liquid. The second interesting point is that the transition to the wetting regime is promoted by increasing the sub-cooling temperature (i.e. [T_{sat} - T_{f0}]). In addition, the prompt break of the curve is also well reproduced by the numerical results highlighting the good behaviour of the updated set of correlations, Eqs. (1)-(4) proposed in this work. However, the numerical results close to ($T_{L,d}$) experience a more abrupt transition than in the experiments. Finally, it should be noted that the transition to the wetting regime occurs at the same ($T_{L,d}$) for all three initial water temperatures (T_{f0}), as reported in Table 2.

6.2 Effects of impacting mass flux

The influence of the impacting mass flux ($\dot{m}$) on the heat flux and surface temperature dependence on time are depicted in Figure 7 for cases 3, 4 and 7 (Table 2). Compared to the experiments, excellent numerical results are obtained in these cases as well. The impact mass flux seems to be the most influential on the wall cooling. Indeed, during the film boiling regime, increasing the impact mass flux results in an increased heat flux. In addition, the transition to the wetting regime at ($T_{L,d}$) was proved to depend also on the impact mass flux ($\dot{m}$), as listed in Table 2. All these dependencies revealed for ($T_{L,d}$) are part of the future modelling challenge.

6.3 Effects of initial wall temperature

The influence of the initial wall temperature (T_{w0}) on the wall heat flux and the surface temperature dependence on time are depicted in Figure 8 for cases 1, 2 and 3 (Table 2). Excellent agreement with experiments was also obtained. Indeed, increasing (T_{w0}), the numerical results have shown similar CHF and surface temperature cooling in the various boiling regimes. The transition to the wetting regime (see the break in the temperature curve, for instance) obviously depends on the input entered by the user for ($T_{L,d}$), which, surprisingly, was proved to depend on the initial wall temperature (T_{w0}), as listed in Table 2. However, such results need to be confirmed in future work.

6.4 Numerical analysis of film formation near the Leidenfrost temperature

Although the Darmstadt database does not include measurements of liquid film characteristics such as thickness, velocity, and temperature, Figures 9, 10, and 11 provide some numerical results when the wall temperature is close to the LFP that could serve as a reference for readers' future work.

Figure 9 shows the liquid film total mass evolution during the transition boiling and nucleate boiling regimes. As expected, the amount of liquid film is sensitive to the impact mass ($\dot{m}$). First, it is shown that it increases with the increasing the impact mass ($\dot{m}$) from 0.9 to 1.6 kg/m^2/s. However, it decreases somewhat by further increasing ($\dot{m}$) to 2.9 kg/m^2/s. This could be due to enhanced splashing and thermal breakup in the latter Case 7. Second, it is found that the amount of liquid film decreases when the subcooling of the injected liquid is reduced in Cases 4,5 and 6.

Figure 10 shows the initial formation of the liquid film at about t=12 s, for Case 7 ($\dot{m}$ = 2.9 kg/m^2/s and *U* = 10.3 m/s). The coloured liquid film by its thickness shows its rapid spreading due to the cooling of the substrate by the droplets of the impacting spray represented as points coloured by theirs sizes.

Finally, Figure 11 shows the impact of the droplets and the evolution of the liquid film thickness on the central area represented in red on Figure 3(b), also for Case 7 ($\dot{m}$ = 2.9 kg/m^2/s and *U* = 10.3 m/s). The spray is represented as spheres proportional to theirs sizes and coloured by their temperatures. Therefore, impinging droplets are bigger and colder. Most of the Lagrangian film parcels are at T_{sat}. These film parcels are clustered together and lead to a wavy liquid film.

Conclusions and future work

This paper includes a brief review and analysis of multidimensional numerical simulations of boiling during droplet jet impact on a heated wall. The state of the art in this field is highlighted and, on this basis, several improvements for the simulation of the boiling of liquid films and spray droplets during their contact with hot walls are proposed. This work has demonstrated that although the simplicity of the current models and correlations, excellent numerical results can be obtained when the user parameters are well calibrated, especially the (T*)-criterion. In this study, various dependencies for ($T_{L,d}$) were revealed, such as to the initial wall temperature and the impact flow rate density, which should be addressed in future work. The key takeaways from this study are:

1. The validation of the proposed models against a unique, complete, and recent experimental database. In particular, the validation of the film boiling model (Eq. (5)) using 3D simulations is the most interesting novelty for CFD software developers. This result motivated the writing of this article because the author believes that the implementation of such a model in current commercial software would be beneficial for various industrial applications.
2. Conjugate heat transfer (CHT) was also found to be an important feature for the simulation of spray-wall interaction and liquid film boiling in the various regimes.
3. Finally, thermal splashing of liquid films transitioning to the Leidenfrost regime should also be implemented and discussed in future work.
4. Additional comparisons with other data are also required.

Acknowledgments

The author would like to thank Prof. Cameron Tropea, Dr. Ilia V. Roisman and Fabian M. Tenzer from the Institute for Fluid Mechanics and Aerodynamics, Technische Universität Darmstadt, Germany for providing complementary information about their experiments. Also, the author would like to thank his colleague Paul-Georgian LUCA for his help on the CONVERGE setup.

Statements and Declarations

- **Funding:** This work has been funded by IFP Energies nouvelles, Institut Carnot IFPEN Transports Energies, 1 et 4 avenue de Bois-Préau, 92852 Rueil-Malmaison, France
- **Competing Interests:** (none)

Reference

[1] A.L.N. Moreira, A.S. Moita, M.R. Panaõ, Advances and challenges in explaining fuel spray impingement: How much of single droplet impact research is useful? Prog Energy Combust. Sci. 36 (2010) 554–580.

[2] V. Bertola, International Journal of Heat and Mass Transfer 85 (2015) 430–437

[3] O'Rourke, P.J. and Amsden, A.A., "A Spray/Wall Interaction Submodel for the KIVA-3 Wall Film Model," SAE Paper 2000-01-0271, 2000. DOI: 10.4271/2000-01-0271

[4] Bai, C. and Gosman, A. "Development of Methodology for Spray Impingement Simulation,"SAE Paper 950283, 1995. DOI: 10.4271/950283

[5] Foucart, H., Habchi, C., Le Coz, J. F., & Baritaud, T. (1998). Development of a three-dimensional model of wall fuel liquid film for internal combustion engines. *SAE transactions*, 60-73.

[6] Habchi, C. "A comprehensive model for liquid film boiling in internal combustion engines." Oil & Gas Science and Technology–Revue de l'Institut Français du Pétrole 65.2 (2010): 331-343. DOI: 10.2516/ogst/2009062

[7] Mundo, C. H. R., Sommerfeld, M., & Tropea, C. (1995). Droplet-wall collisions: experimental studies of the deformation and breakup process. International journal of multiphase flow, 21(2), 151-173.

[8] Moreira, A. L. N., Moita, A. S., Cossali, E., Marengo, M., & Santini, M. (2007). Secondary atomization of water and isooctane drops impinging on tilted heated surfaces. Experiments in Fluids, 43(2), 297-313.

[9] Liu, Y., et al. "Evaporation time and vapor generation limit of a droplet on a hot surface." International Journal of Heat and Mass Transfer 173 (2021): 121280.

[10] Hidaka, S., Takata, Y., Yamamoto, H., Yamashita, A., & Ito, T. (2003). Wettability and droplet evaporation on plasma-irradiated metal surface. Nippon Kikai Gakkai Ronbunshu, B Hen/Transactions of the Japan Society of Mechanical Engineers, Part B, 69(678), 437-444.

[11] Chang Cai, Issam Mudawar, Hong Liu, Chao Si, Theoretical Leidenfrost point (LFP) model for sessile droplet, International Journal of Heat and Mass Transfer, Volume 146, 2020, 118802, ISSN 0017-9310, https://doi.org/10.1016/j.ijheatmasstransfer.2019.118802.

[12] Testa, P., & Nicotra, L. (1986). Influence of pressure on the Leidenfrost temperature and on extracted heat fluxes in the transient mode and low pressure.

[13] Celata, G. P., Cumo, M., Mariani, A., & Zummo, G. (2006). Visualization of the impact of water drops on a hot surface: effect of drop velocity and surface inclination. *Heat and mass transfer*, *42*(10), 885-890.

[14] Tenzer, F., Roisman, I., & Tropea, C. (2019). Fast transient spray cooling of a hot thick target. Journal of Fluid Mechanics, 881, 84-103. doi:10.1017/jfm.2019.743

[15] Junseok Park, Hyungdae Kim, Direct-contact heat transfer of single droplets in dispersed flow film boiling: Experiment and model assessment, Nuclear Engineering and Technology, 2021, https://doi.org/10.1016/j.net.2021.02.017.

[16] van Limbeek, Michiel AJ, et al. "Vapour cooling of poorly conducting hot substrates increases the dynamic Leidenfrost temperature." *International journal of heat and mass transfer* 97 (2016): 101-109.

[17] Tenzer, F. M., Hofmann, J., Roisman, I. V., & Tropea, C. (2020). Leidenfrost temperature in sprays: role of the substrate and liquid properties. *arXiv preprint arXiv:2001.05426*.

[18] Siemens, 2018. Siemens Product Lifecycle Management Software Inc., Simcenter STAR-CCM+ Documentation, Version 13.04.

[19] Richards, K.J., Senecal, P.K., and Pomraning, E., CONVERGE 3.0, Convergent Science, Madison, WI (2020).

[20] Kuhnke, D., "Spray/Wall-interaction Modelling by Dimensionless Data Analysis," Ph.D. Thesis, Shaker Verlag, 2004, ISBN 3-8322-3539.

[21] Castanet, G., Chaze, W., Caballina, O., Collignon, R., & Lemoine, F. (2019, September). Drop impact in the regime of film boiling transient evolution of the heat transfer and the vapor film thickness. In *29th Conference on Liquid Atomization and Spray Systems*. https://hal.archives-ouvertes.fr/hal-02388412/document

[22] Breitenbach, J., Roisman, I. V., & Tropea, C. (2017). Heat transfer in the film boiling regime: Single drop impact and spray cooling. *International Journal of Heat and Mass Transfer*, *110*, 34-42.

[23] Rohsenow, W.M., 1952. A method of correlating heat transfer data for surface boiling liquids. J. Heat Transfer (74), 969–976.

[24] J.H. Lienhard, A Heat Transfer Textbook, 4th edition (https://ahtt.mit.edu/).

[25] Lienhard, J. H., and V. K. Dhir. "Hydrodynamic prediction of peak pool-boiling heat fluxes from finite bodies." (1973): 152-158.

[26] Börnhorst, M., Kuntz, C., Tischer, S., & Deutschmann, O. (2020). Urea derived deposits in diesel exhaust gas after-treatment: Integration of urea decomposition kinetics into a CFD simulation. *Chemical Engineering Science*, *211*, 115319.

[27] Wruck, N.M. and Renz, U., "Transient Phase-Change of Droplets Impacting on a Hot Wall,"Wiley-VCH Verlag GmbH, ISBN 978-3-527-27149-8.

[28] G. Liang, I. Mudawar, Review of spray cooling - Part 1: single-phase and nu- cleate boiling regimes, and critical heat flux, Int. J. Heat Mass Transf. 115 (2017) 1174–1205, doi:10.1016/j.ijheatmasstransfer.2017.06.029

[29] G. Liang, I. Mudawar, Review of drop impact on heated walls, Int. J. Heat Mass Transf. 106 (2017) 103–126, doi: 10.1016/j.ijheatmasstransfer.2016. 10.031

Table 1: Initial and boundary conditions		
Gas	Solid	Spray injection
Air Y_{N2}=0.75 Y_{O2}=0.21 Y_{CO2}=0.04 T_0 = 300 K P_0 = 1 atm	Stainless steel ρ_w = 7900 kg/m^3 $C_{p,w}$ = 477 J/(kg*K) λ_w = 14.9 W/(m*K) T_{w0} = 622-723 K Surface roughness = 0.03 µm Adiabatic except the top face	Water Continuous injection Full cone angle = 45° Measured mean droplets size: D_{10} = 43 – 64 µm Measured impact velocity: U = 8 – 10.3 m/s Measured flow rate at the wall location: $\dot{m}$ = 0.9 – 2.9 kg/m^2/s

Table 2: Simulations parameters and boundary conditions						
Case #	$\dot{m}$ [kg/m^2/s]	U [m/s]	D_{10} [µm]	T_{w0} [K]	T_{f0} [K]	$T_{L,d}$ [K]
1	1.6	8	64	623	313	545
2				673		548
3				723		576
4	0.9	9.9	43	723	313	610
5					332	
6					352	
7	2.9	10.3	55	723	313	580

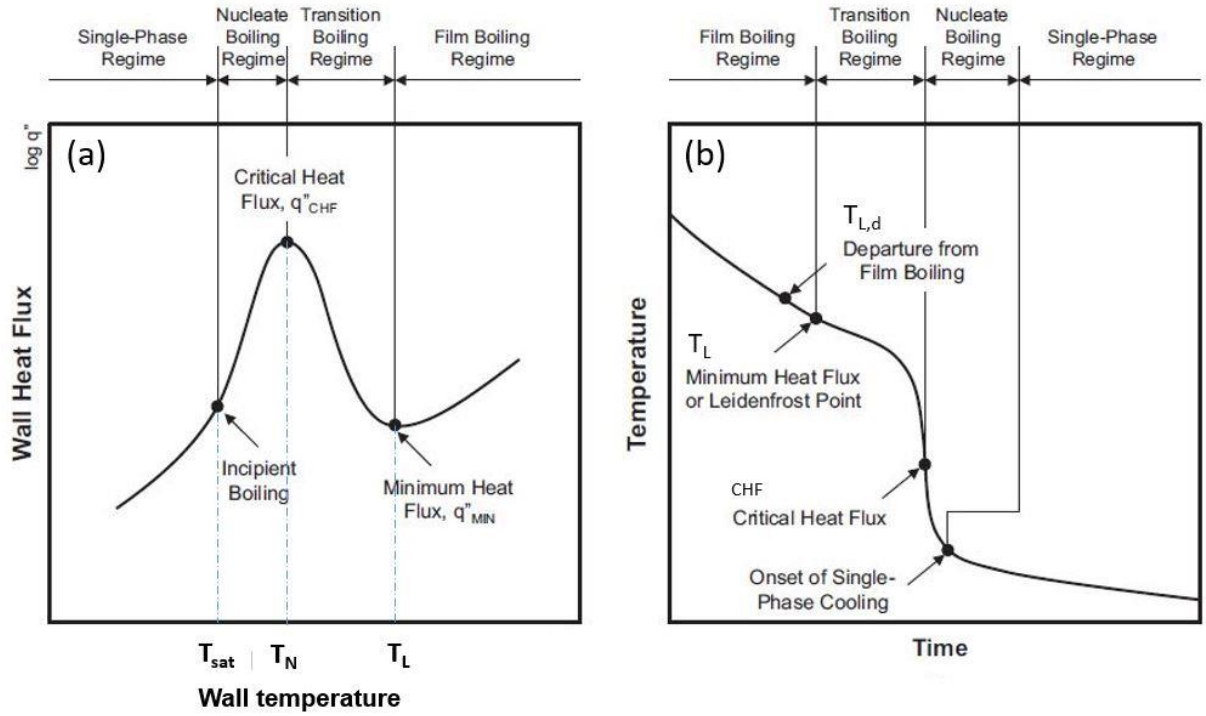

Figure 1: (a) Boiling and evaporation curves, and (b) quench curve associated with a drop or a spray impinging a hot wall. Modified and adapted from Liang and Mudawar [28].

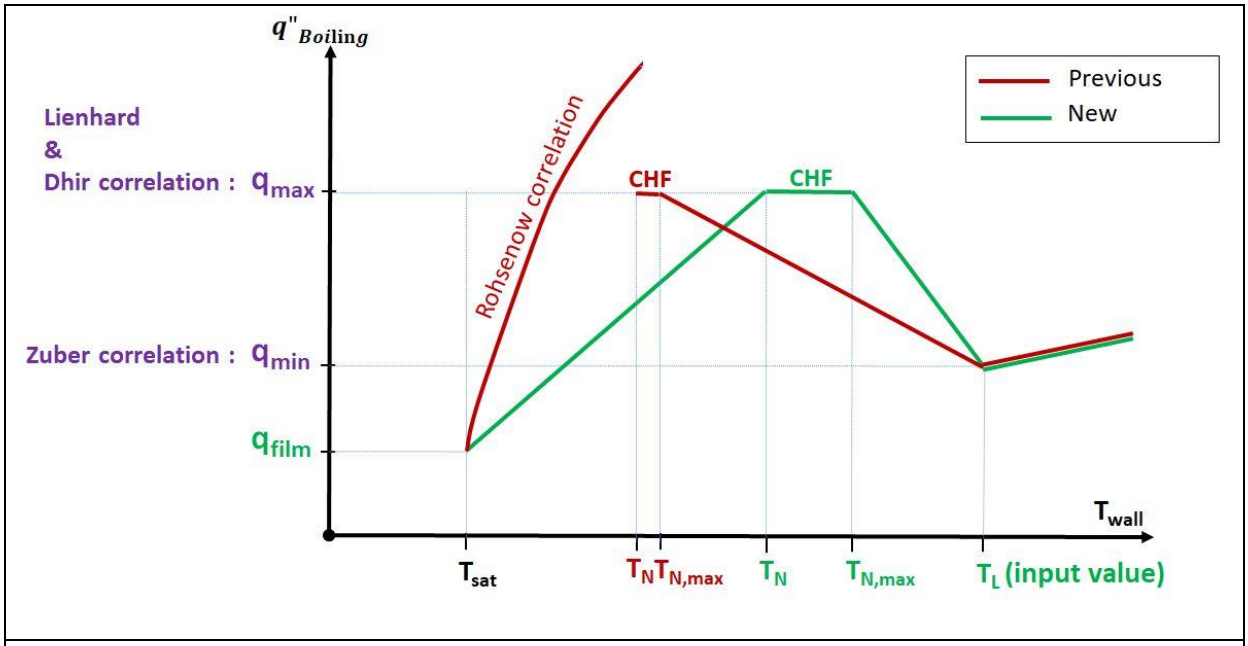

Figure 2: Updated and previous wall heat fluxes modelling in the nucleate boiling, transition boiling, and Leidenfrost boiling regimes for a liquid film already formed on the wall.

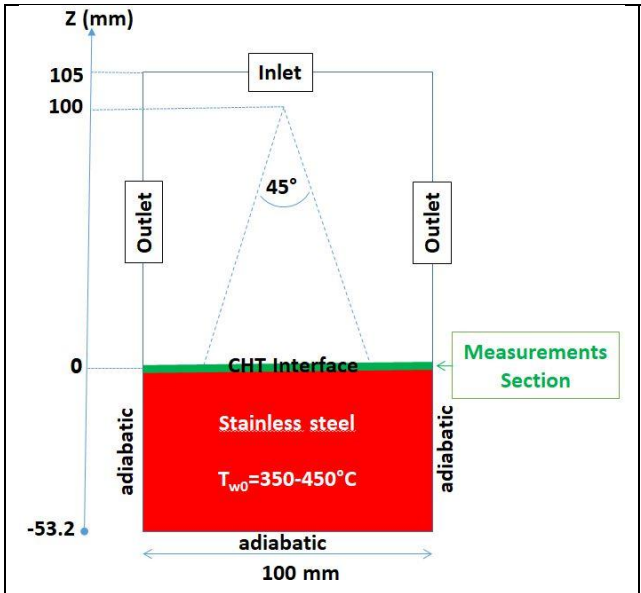

(a) Schematic of the experiments along with the operating and boundary conditions. The numerical setup considers conjugate heat transfer (CHT) at the wall surface (in green).

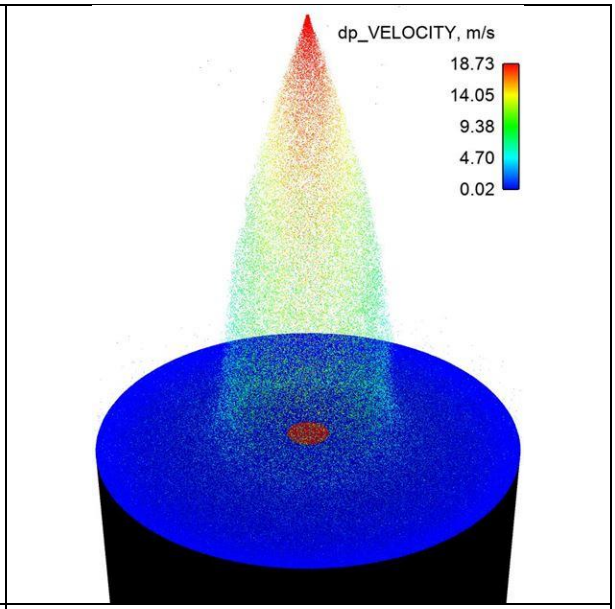

(b) A numerical result showing the spray impacting the heated wall. Central boundary (in red with D = 10 mm) for results post-processing.

Figure 3: Main characteristics of the Darmstadt experiments [6].

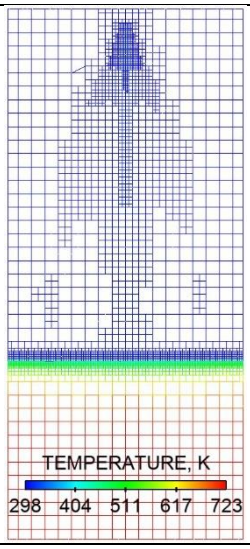

Figure 4: Mesh (2D cut) showing the various embedding near the impacted wall in the gas and solid sides at t=20s for Case 7 ($\dot{m}$ = 2.9 kg/m^2/s and *U* = 10.3 m/s). The AMR is also shown for the spray. The base grid is equal to 4 mm in the solid region and 1 mm in the gas region. Three fixed embedding were specified. The first one with 0.5 mm grid size is located downstream of the injector nozzle (at the top, as shown in Figure 3). The other two, with a 0.25 mm grid, are located on either side of the substrate surface. With this refinement strategy, the total number of cells is between 5 and 9 million during runtime. The CPU time is 765 seconds per second computed on 360 cores of the latest generation Intel Skylake G-6140 processors running at 2.3 GHz (ENER440 IFPEN Supercomputer).

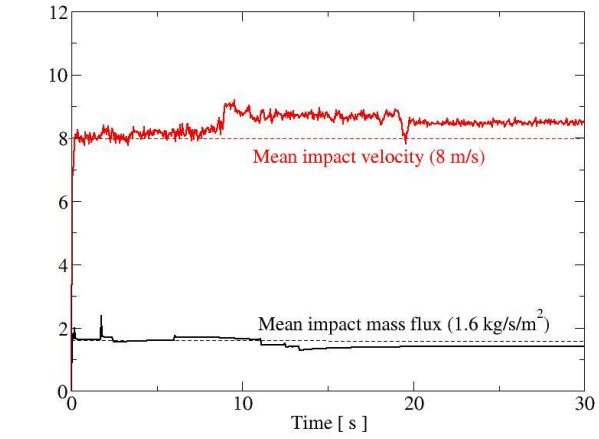

(a) Case 3: $\dot{m}$ =1.6 kg/m^2/s and *U* = 8 m/s

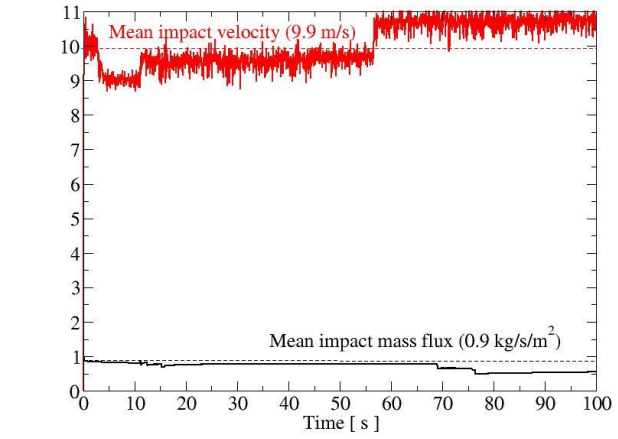

(b) Case 4: $\dot{m}$ =0.9 kg/m^2/s and *U* = 9.9 m/s

Figure 5: Validation of the numerical impact conditions of the spray on the central part of the substrate corresponding to the nominal experimental impact conditions. Two set of data are included in these figures: mean impact velocity ((*U*) in red) and mean impact mass flux (($\dot{m}$) in black).

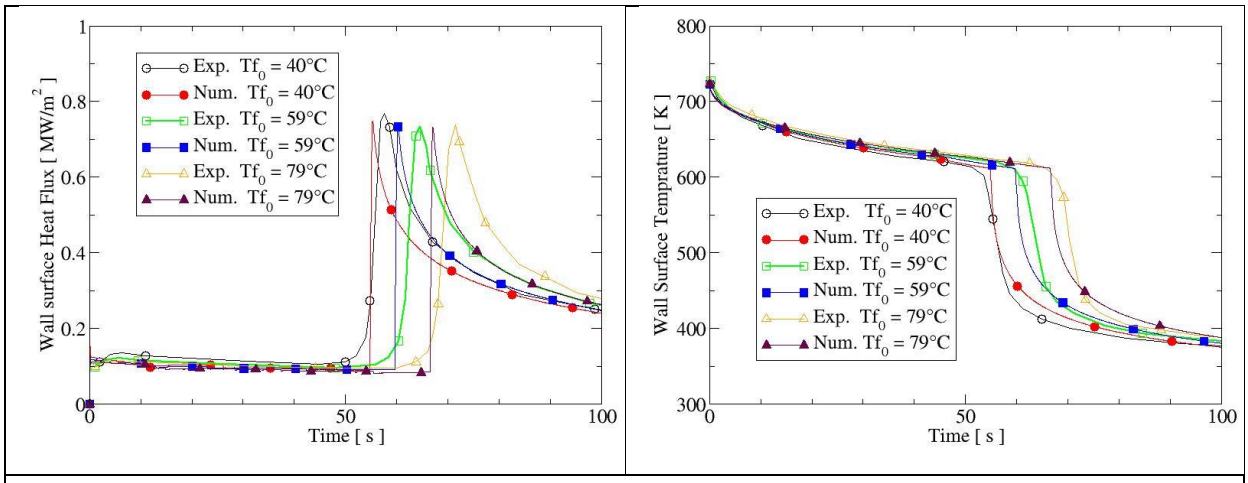

Figure 6: Effects of liquid injection temperature, T_{f0} (Cases 4, 5 and 6, see Table 2). Flow rate density, $\dot{m} = 1.6\ kg/(m^2.s)$.

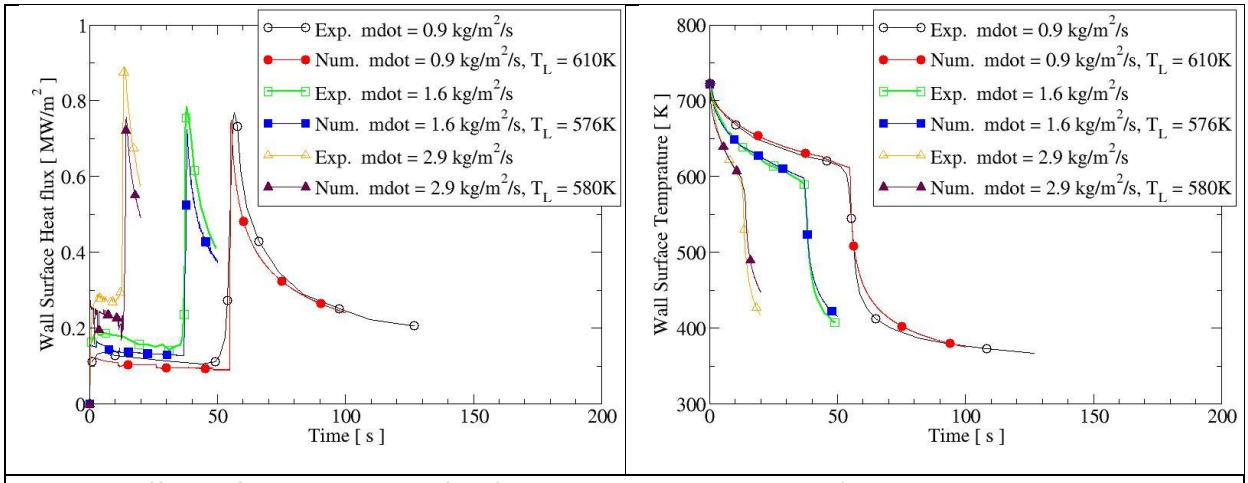

Figure 7: Effects of impacting mass flux (Cases 4, 3 and 7, see Table 2). T_{w0} = 450 K. In the caption, the mass flow rate density, $\dot{m}$ is denoted mdot.

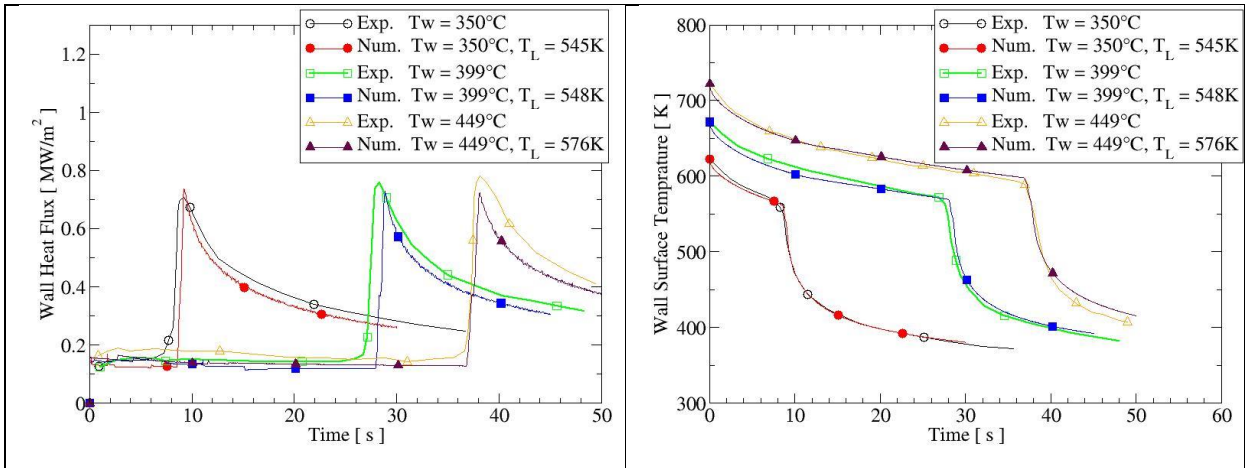

Figure 8: Effects of initial wall temperature (Cases 1, 2 and 3, see Table 2).

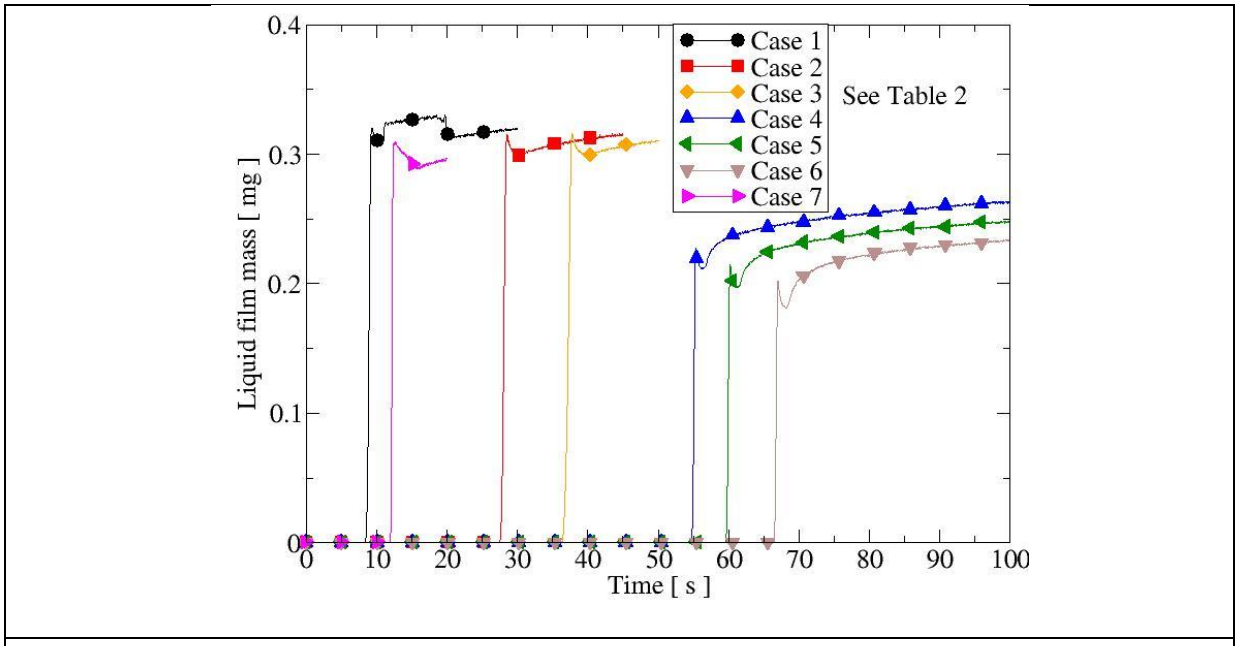

Figure 9: Liquid film total mass evolution during the transition boiling and nucleate boiling regimes.

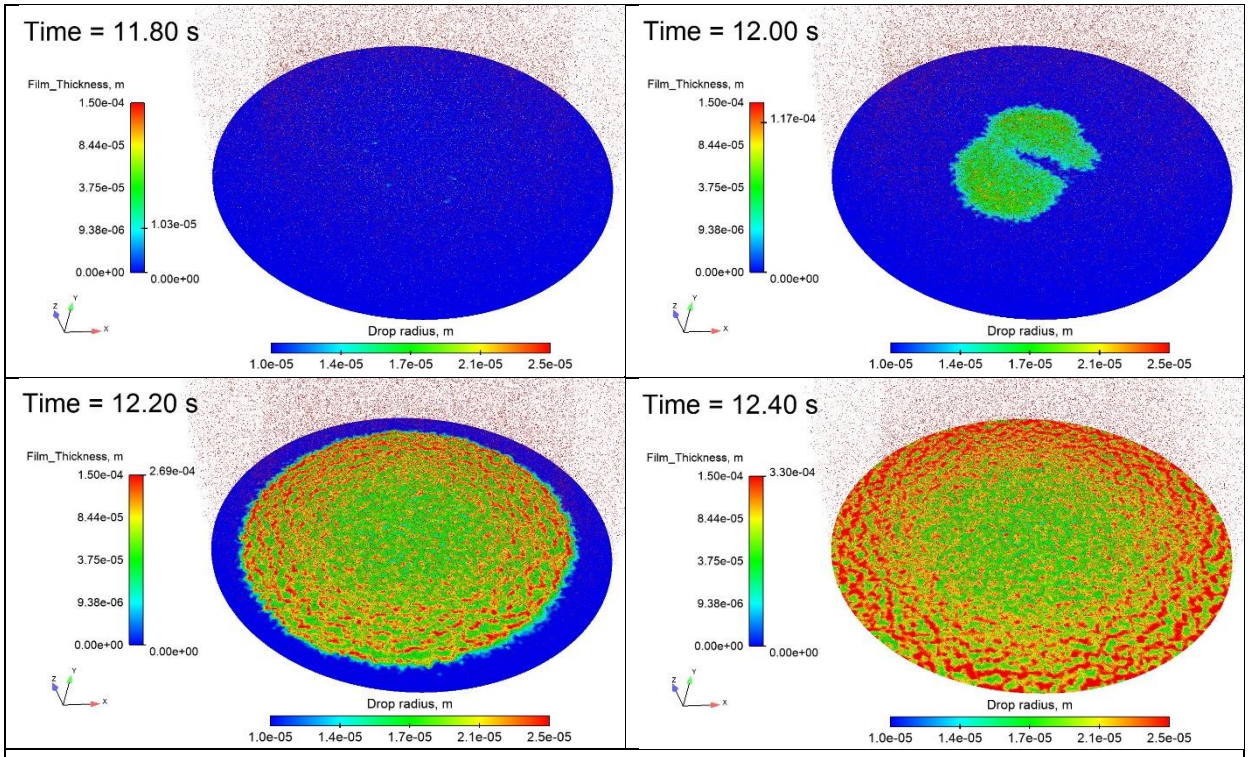

Figure 10: Formation of a liquid film and subsequent spreading due to cooling of the substrate by the impinging spray droplets for Case 7 ($\dot{m}$ = 2.9 kg/m^2/s and U = 10.3 m/s). Le liquid film is coloured by the its thickness. The impinging spray droplets are represented as points coloured by theirs sizes.

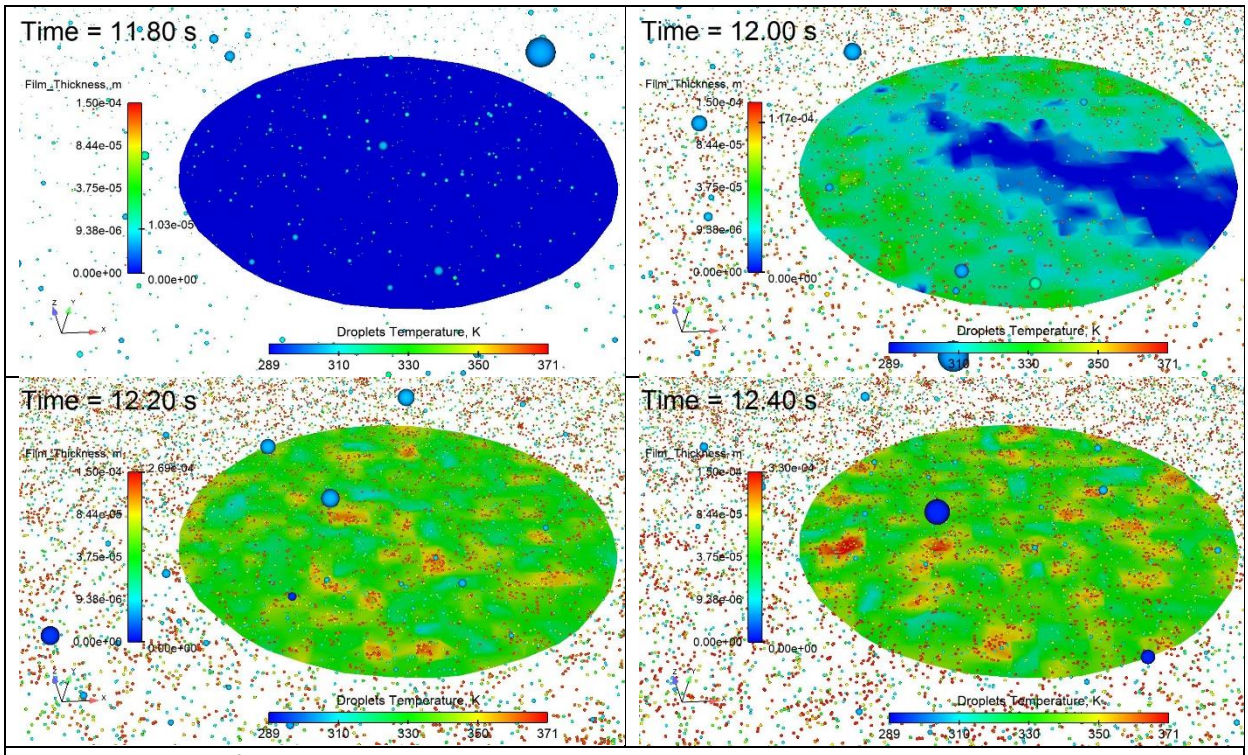

Figure 11: Liquid film thickness evolution on the substate due to the spray impingement; Zoom on the impact zone show in red in Figure 3. Case 7 ($\dot{m}$ = 2.9 kg/m^2/s and U = 10.3 m/s). The spray is represented as spheres proportional to theirs sizes and coloured by their temperatures. Therefore, impinging droplets are bigger and colder. Most of the Lagrangian film parcels are at T_{sat}. These film parcels are clustered together and lead to a wavy liquid film.